Investigation of a Size-Selective Single Hafnium-Encapsulated Germanium Cage

Jin Wang,* Xing Chen, and Jin Huai Liu

Institute of Intelligent Machines, Chinese Academy of Sciences, Hefei, 230031, AnHui, P. R. China

Received: May 20, 2008; Revised Manuscript Received: July 3, 2008

The structures, relative stabilities, and electronic properties of size-selective single Hf-encapsulated germanium caged clusters ($n = 9-24$) have been investigated in detail by density functional method for the first time. The dominant growth behavior of the solid nanocluster Hf@Ge_n is based on a pentagonal prism instead of a hexagonal prism. Analogous to Hf@Si_n, the encapsulated fullerene-like structure of Hf@Ge_n begins to appear at 14, which is consistent with the prediction from the reactivity toward water in a recent experiment (*J. Phys. Chem. A* **2007**, *111*, 42). Also, similar to Hf@Si_n in the previous experimental observation (*Chem. Phys. Lett.* **2003**, *371*, 490), the binding energy of Hf@Ge_n is gradually increased up to the maximum at 16 and tends to be decreased subsequently, suggesting that stabilization of large germanium cages needs to be realized by doping more Hf atoms. The encapsulated Hf will obviously be moved away from the center of the germanium cage if the cluster size of Hf@Ge_n is larger than 20. According to analysis of the electron density of size-selective Hf@Ge_n, the covalent character in the germanium framework can be affected by the encapsulated position of Hf in the germanium cage. In addition, comparison between typical low-lying size-selective Hf@Ge_n and Hf@Si_n ($n = 12$, 16 and 20) cages indicates that large-scaled divergence exists in stabilities, growth behaviors, electronic properties, and so forth.

1. Introduction

Recently, the properties and functionalization of various novel semiconductor nanomaterials have been widely investigated because they are important for their application as semiconductor devices, sensors, and so forth. However, understanding of properties such as structure, electron properties, and so forth is difficult to obtain via experimental approach. In contrast, information of geometries or electron properties can be obtained by ab initio or density functional theory. A size-selective semiconductor germanium cluster with transition metallic impurity is currently of great interest because of its magic numbers in stabilities for building blocks of nanomaterials, tunable highest occupied molecular orbital−lowest unoccupied molecular orbital (HOMO−LUMO) gaps for application in sensors or absorption of luminescence at the nanoscale for biological systems, strong sized selectivity, and magnetism for assembly of magnetic nanodevices.[1–11] As for Co-doped semiconductor germanium clusters, bicapped tetragonal antiprism Ge_{10} is the best cage with extraordinary stability;[12] however, in the case of Zn, an icosahedral prism is an appropriate building block for assembly.[13] On the basis of the hexagonal antiprism of a $MnGe_{12}$ cluster, the hexagonal antiprism units could be repeated to form finite or infinite stacked hexagonal structures and develop nanotubes of Ge doped with Mn, indicating that these nanotubes are interesting as nanomagnets or nanosensors.[14] So far, discussions about the growth behavior of metal-doped semiconductor nanoclusters mainly focus on cluster sizes lower than 16.[15–17] Very limited structures of metal encapsulated germanium or silicon clusters at $n = 16$, 18, or 20, e.g., fullerene-like and close-packed structure have been found in recent computational work.[18–21] Furthermore, structures of metal encapsulated germanium clusters with sizes of >20 have not been investigated in detail. Additionally, recent investigation suggests that some divergences between MGe_n ($n = 12$ and 10) and MSi_n ($n = 12$ and 10) could be found.[6] Therefore, it is interesting to thoroughly investigate the growth behavior of metal encapsulated germanium clusters at the wide range from 10 to 24 and search novel appropriate building blocks for the assembly of three-dimensional (3D) structures such as solid C_{60}.

2. Computational Details

The geometry of size-selective Hf@Ge_n ($n = 9-24$) clusters are optimized via unrestricted density functional theory (DFT/B3LYP) combined with effective core potential LanL2DZ basis sets.[22–24] The standard LanL2DZ basis sets could be effective in calculating transition metal in 5d series because the difficulty of two-electron integrals from heavy transition metal atom is efficiently overcome. Moreover, the LanL2DZ basis sets were proven to be reliable in the previous investigations of transition metal (TMA) doped silicon and germanium (TMA@Si_n and TMA@Ge_n) systems.[5,6] Herein, in order to test the reliability of our calculations, Hf_2 dimer is calculated using UB3LYP/LanL2DZ. The theoretical results suggest that the triplet Hf_2 dimer is the most stable state and its vibrational frequency is 187.5 cm^{-1}, which is in agreement with the experimental value of 176.2(26) cm^{-1} in the resonance Raman spectrum of mass-selected Hf_2 dimer.[25] All the theoretical calculations are performed with the Gaussian 03 program package.[26] The numerous initial isomers are based on a number of known single TMA@Ge_n in previous works through the insertion pattern of Hf in caged germanium clusters[27] or the capping pattern of Ge in the low-sized Hf@Ge_n precursor.[5] In order to test the reliability of the optimization approach, different density functional methods, e.g., B3PW91 and B3P86, are also employed for optimization of some low-lying isomers of Hf@Ge_n. The calculated results suggest that the geometries, stabilities, and electronic properties of these competitive species are not obviously changed using different optimization methods. On the basis of the optimized structures of the lowest-energy

* Author to whom correspondence should be addressed. E-mail: jwang@iim.ac.cn. Fax: +86-551-5592420.

10.1021/jp804433d CCC: $40.75
Published on Web 08/23/2008

isomers with different spin states, the results indicate that the spin singlet state of the Hf@Ge_n cluster are the lowest-energy geometries compared to spin triplet and quintet states.

3. Results and Discussion

3.1. Geometries of Size-Selective Hf@Ge_n ($n = 9-17$). Previous investigation of single TMA-doped germanium clusters suggested that the position of TMA gradually began to transform from the surface site of germanium framework to the inner site at $n = 9$.[5] Therefore, the present investigation of a germanium cluster with a single Hf impurity mainly focuses on the encapsulation of Hf in a germanium cage from the cluster size of $n = 9$. As shown from optimized geometries of $HfGe_9$ in Figure 1, the doping pattern of Hf in Ge_9 clusters could be observed as Hf concaved in a Ge_9 framework. For example, concaved $HfGe_9$ 9a isomer is lower in total energy than 9c and 9d with doping of Hf on the surface of a germanium framework by 0.24 eV and 0.40 eV, respectively. Different from the bicapped tetragonal antiprism of TMA@Ge_{10} (TMA = Cu, Ni, and Co) as the most stable structure,[5,12] the total electronic energy of cubic isomer 10a is obviously lower than those of other isomers, e.g., pentagonal prism 10c, and so forth, suggesting that the thermodynamic stability of the Hf concaved cubic structure is relatively strong. Similar to $HfGe_{10}$, cubic isomer 11a, which is evolved from 10a by capping of Ge, is quite lower in total energy than the other isomers. As observed from the stable structures of $HfGe_{11}$, the capped pentagonal antiprism 11b is the second lowest-energy isomer in all the located isomers, which is different from $CuGe_{11}$.[5] Previous investigation of single TMA-doped Si_{12} caged clusters revealed that the hexagonal prism was the lowest-energy structure and could act as the approximate building block of stacked one-dimensional (1D) TMA-encapsulated germanium nanotubes.[14,28–30] Compared to pure Ge_{12} with a distorted icosahedron as the lowest-energy structure,[27] the lowest-energy isomer of Hf@Ge_{12} is also located as hexagonal prism 12a; however, its high symmetry is broken and appears as irregular geometry with different bond lengths of Ge−Ge and Hf−Ge. The multirhombii 12d and the capped pentagon-hexagonal prism 12c are also found as high-energetic isomers compared to hexagonal prism 12a. Obviously, the lowest-energy conformer, viz., face-capped hexagonal prism Hf@Ge_{13} 13a could be formed from the addition of Ge on the hexagonal prism Hf@Ge_{12} 12a, whereas the addition of Ge on the rhombus could lead to another high-energy isomer 13d. If the 13th Ge atom is edge-capped on the hexagonal prism Hf@Ge_{12} 12a, two almost isoenergetic isomers 13b and 13c could be formed; moreover, their total electronic energies are only higher than that of 13a by 0.02 eV and act as candidates of the ground-state of Hf@Ge_{13}. When the cluster size of Hf@Ge_n is increased up to 14, the smallest fullerene-like structure Hf@Ge_{14} 14a begins to be formed, and its total energy is lower than the other located isomers. On the basis of the hexagonal prism Hf@Ge_{12}, bicapped Ge atoms on rhombii can result in the formation of the low-lying isomer 14b. Also, different capping patterns of Ge atoms on hexagonal prisms can form different stable conformers 14d and 14e. It should be noted that bicapped Ge atoms on an icosahedral prism leads to form the stable structure 14c; however, its total energy is relatively higher than that of 14a by 0.52 eV. Different from Hf@Ge_{14}, although the fullerene-like isomer of Hf@Ge_{15} could be located as minima, e.g., 15b, 15e, and 15f, the lowest-energy isomer 15a, which is developed from a pentagonal prism by edge-capping of Ge atoms, is quite lower in total energy than the other isomers. In addition, the independent capping pattern of Ge on pentagonal prisms can yield the high-energy isomer 15c compared to 15a, implying that the stabilities of the prismatic cage based on the identical precursors is obviously influenced by the capping pattern and position of germanium atoms. Similar to Hf@Ge_{13} and Hf@Ge_{14}, stable isomer 15i can also be formed from the initial hexagonal prism by the tricapping pattern of germanium atoms. For a Hf-encapsulated Ge_{16} cage, fullerene-like Hf@Ge_{16} appears as a low-lying isomer, and it is composed of eight pentagons and two rhombii; however, its stability is relatively weaker than that of 16a evolved from a pentagonal prismatic precursor, in that its total electronic energy is higher than 16a by 0.24 eV. It should be mentioned that one high-lying isomer 16f is formed by tetracapped germanium on a hexagonal prism; however, its stability is quite weaker compared to that of 16a because its total electronic energy is much higher than 16a by 1.11 eV, implying that the stability of a hexagonal prism is relatively more stable in contrast to a pentagonal prism, and extra addition of a germanium atom on the hexagonal prism is more difficult. Guided by the fullerene-like Hf@Ge_{16} 16b, the analogous fullerene-like Hf@Ge_{17} 17a is found as the lowest-energy isomer in all the located isomers, indicating that the formation of a fullerene-like structure at the cluster size $n = 17$ is more favorable than the smaller clusters. As mentioned above, the hexagonal prism is unfavorable to form large caged clusters through the addition of extra germanium atoms. Again, the high-lying isomer 17d with higher total energy (0.63 eV) than that of 17a is obviously evolved from Hf@Ge_{16} 16f. Similar to Hf@Ge_{15} and Hf@Ge_{16}, two stable isomers 17f and 17g, which are based on a pentagonal prism, can also be located. On the basis of analysis of the structures and stabilities of Hf@Ge_n ($n = 9-17$) caged clusters, it is concluded that the derivative pattern on a pentagonal prismatic precursor is superior to that on a hexagonal prismatic precursor; moreover, the smallest fullerene-like structure appears from $n = 14$ and gradually becomes another dominant evolvement pattern with increase of the size of caged cluster Hf@Ge_n. In contrast, layer structures of pure Ge_n ($n = 13-17$) were suggested as the lowest-energy isomers in the previous calculations,[27] suggesting that Hf doping in a germanium framework could cause the deformation of germanium geometry.

3.2. Geometries of Size-Selective Hf@Ge_n ($n = 18-24$). A number of initial caged structures of Hf@Ge_{18} are considered, and different energy isomers (see Figure 2) could be located as minima. The lowest-energy and the second-lowest-energy isomer 18a and 18b are yielded from circular capping of eight germanium atoms around a pentagonal prism and the addition of germanium atoms on the fullerene-like cage, respectively. Additionally, fullerene-like 18h and 18i can be formed by different addition patterns of germanium atoms on fullerene-like Hf@Ge_{16} 16b, that is, the rhombus is changed to be a folded hexagonal ring in 18i, while the optimized structure of 18h shows that the rhombus in 16b is transformed to be folded pentagons. It should be pointed out that novel fullerene-like cage 18k could be found as a stable structure, and it can be described as circular capping of eight germanium atoms on the pentagonal antiprism. On the other hand, isomer 18e is formed by circular capping of eight germanium atoms on the pentagonal prism and is more favorable because of its relatively strong stability, which is reflected by its lower total electronic energy that that of 18k by 0.4 eV. Although isomer 18c based on a hexagonal prism is located as a stable structure, its total electronic energy is obviously higher than that of 18a by 0.53 eV, indicating that circular capping of extra germanium atoms on the hexagonal

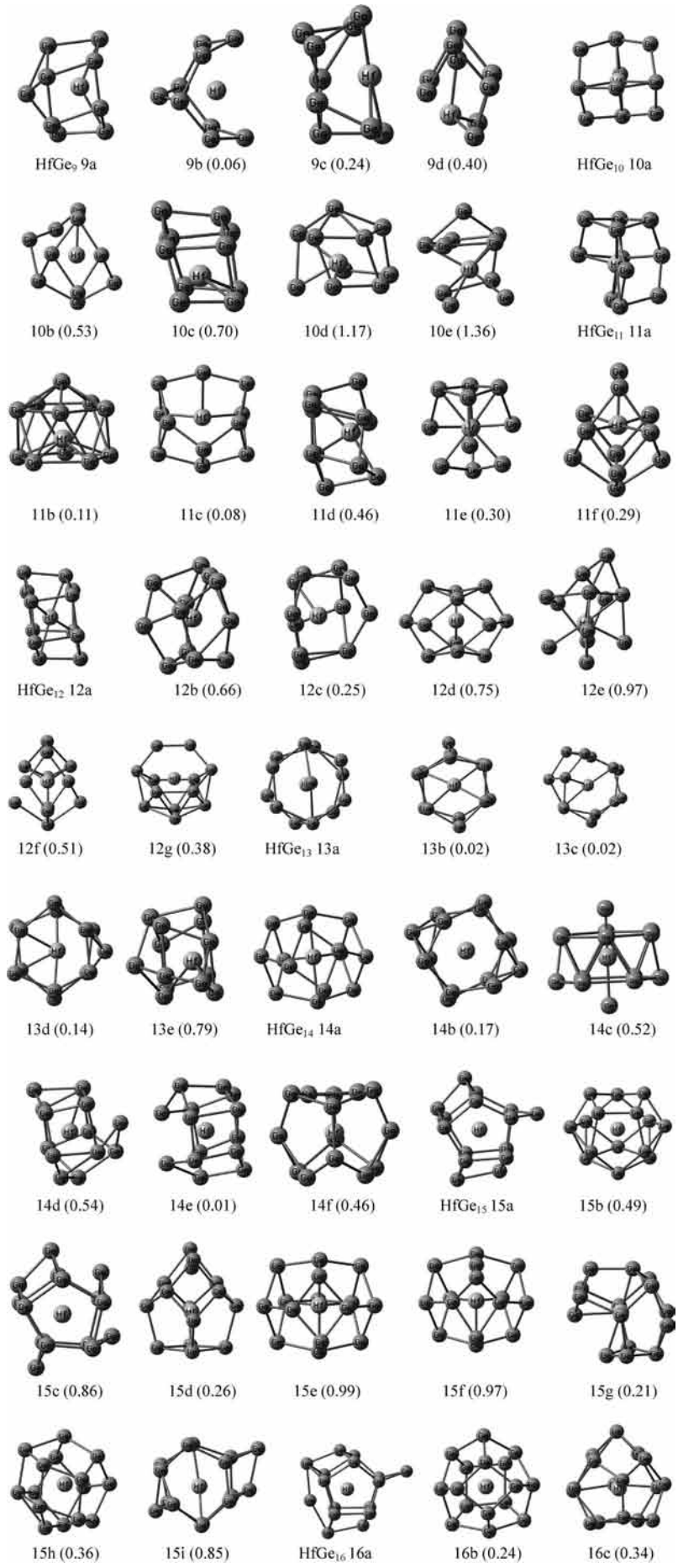

Figure 1. Part 1 of 2.

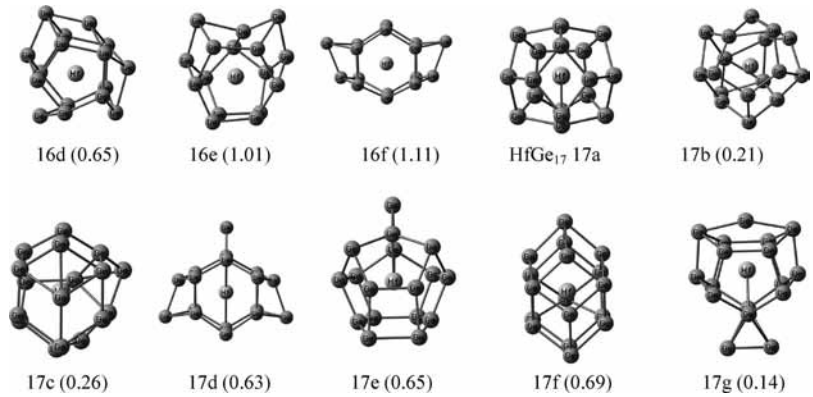

Figure 1. Part 2 of 2. The equilibrium structures of size-selective Hf@Ge$_n$ (n = 9−17). The relative energies (in eV) of the different isomers at the different sizes are shown in parentheses.

prism is not favorable at this size. As seen from the optimized results, the caged structure of Hf@Ge$_n$ is quite complicated and quite a number of irregular deformed geometries could be found as stable isomers. As far as the caged cluster of Hf@Ge$_{19}$ is concerned, the lowest-energy and second-lowest-energy isomer 19a and 19b can be developed from the circular capping of nine germanium atoms on the staggered pentagonal prism. Three isomers 19d−f, which are evolved from circular capping of germanium atoms around a hexagonal prism, can be found as stable structures. Similar to Hf@Ge$_{18}$, two high-lying isomers 19i and 19k are formed by circular capping of nine germanium atoms on the pentagonal antiprism. When the cluster size of caged Hf@Ge$_n$ is up to 20, a large number of initial structures are considered, and more than 20 isomers are suggested as stable structures according to analysis of vibrational frequencies. It should be mentioned that the dodecahedral structure of Hf@Ge$_{20}$ is located as the second-lowest isomer in all the located isomers, and the optimized structure can be formed through circular capping of 10 germanium atoms on the pentagonal antiprism. On the basis of fullerene-like Hf@Ge$_{16}$ 16b, the analogous fullerene-like 20a with asymmetrical capping of four germanium atoms can be found as the lowest-energy isomers in all the located isomers and the nondirect interaction between the four germanium atoms and Hf, which indicates that the outer germanium layer can be formed at this size in the dominant optimized structure. Some other complicated caged structures, e.g., 20d and 20h, can be observed as the derivatives from the small fullerene-like Hf@Ge$_{16}$ 16b. One stable isomer 20k, which is formed via capping of eight germanium atoms surrounded by a hexagonal prism, is indicated as the high-lying isomer with the fairly high total electronic energy compared to the dodecahedral isomer. Additionally, one pyramid-like isomer 20i is also suggested as a high-lying stable structure. In comparison with previous investigations of single TMA encapsulated germanium isomers that only focused on cluster sizes lower than 20, the geometries and stabilities of caged cluster sizes of Hf@Ge$_n$ larger than 20 is also studied in detail. On the basis of dodecahedral isomer Hf@Ge$_{20}$ 20b, the most stable structure of Hf@Ge$_{21}$ 21a can be yielded via capping of Ge atom; furthermore, the position of Hf is moved away from the center of the germanium cage. Also, some irregular cages based on pentagonal antiprism, e.g., 21c, 21d, and 21f, could be found as different energetic isomers by asymmetrical capping of germanium atoms. One low-lying isomer 21g can be described as a square germanium framework capping on the rhombus in fullerene-like Hf@Ge$_{16}$ 16b to form the second layer and the face-capping of the 21st germanium atom on the square germanium framework to form outer-layer and indirect interaction with Hf. The high-lying isomer 21e can be depicted as 11 germanium atoms capped on the folded hexagonal−pentagonal prism. Analogous to the Hf@Ge$_{21}$, the lowest-energy and second-lowest-energy isomer of Hf@Ge$_{22}$ 22a and 22b are formed from capping of Ge on the dodecahedral Hf@Ge$_{20}$ 20b; furthermore, their total electronic energies are very close, indicating that the two isomers are the most possible candidates for the ground-state of Hf@Ge$_{22}$. According to optimized results on geometries of Hf@Ge$_{22}$, the formation of many low-lying isomers could be based on the dodecahedral precursor. For example, low-lying 22e and 22f are formed through the edge-insertion pattern of two germanium atoms at different surface sites of the dodecahedral cage. As far as the lowest-energy isomers of Hf@Ge$_{23}$ and Hf@Ge$_{24}$ caged clusters are concerned, some extra germanium atoms are capped on the dodecahedral cage to form an outer layer without direct interaction with Hf. It should be noted that when the size of Hf@Ge$_n$ exceeds 20, the metal impurity Hf obviously deviates from the center of the dodecahedral cage and only directly interacts with a partial germanium framework.

3.3. Relative Stability of Size-Selective Hf@Ge$_n$ Clusters. In order to predict relative stabilities of the Hf@Ge$_n$ cluster, it is important to calculate the fragmentation energy and the second-order energy difference.

As shown in Figure 3, it is suggested that the average binding energy of size-selective clusters is gradually increased to a maximum at the size of 16, then the average binding energy tends to decrease with the increase of cluster size. Therefore, it can be expected that the high binding energy of Hf@Ge$_{16}$ is related to the germanium-capped pentagonal prismatic cage and sealed Hf-encapsulated fullerene-like cage, with the Hf impurity located at the center of the germanium cage. The fragmentation energies and the second-order energy difference of size-selective Hf@Ge$_n$ reveal that local maxima appear at 10, 12, 15, 16, 18, 20, and 23, which is somewhat different from the local maxima of pure Ge$_n$ at 10, 14 16, 18, 21, and 23.[27] The special stability of Hf@Ge$_{10}$ compared to its neighbors is in agreement with the previous experimental observation and theoretical results.[5,12] As far as the strong stability of Hf@Ge$_{12}$ is concerned, it is mainly related to the hexagonal prism, which is analogous to the experimental observation of TMA@Si$_{12}$.[1] As far as the large caged clusters are concerned, their relatively special stabilities at specific size are related to the geometries of the competitive species of the ground state. For example, the special stability of Hf@Ge$_{20}$ could be related to the fullerene-like structure as

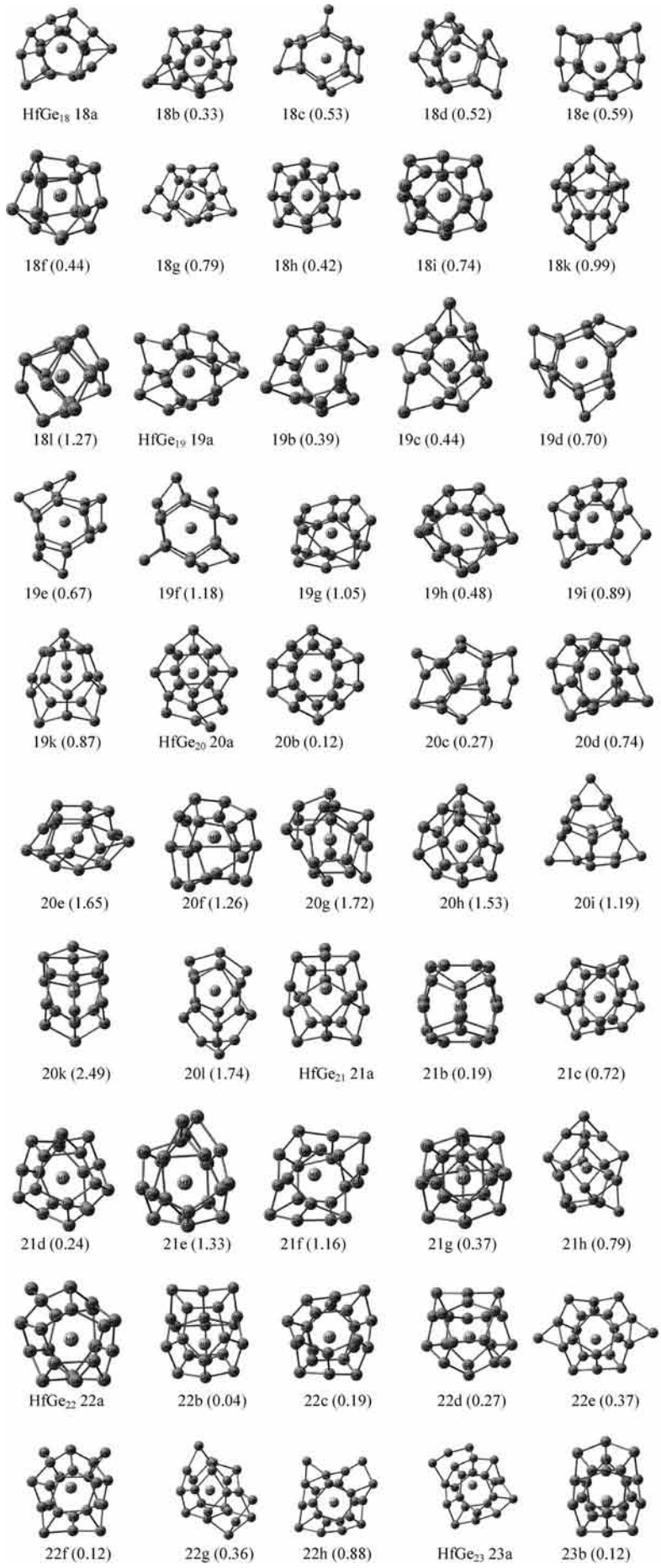

Figure 2. Part 1 of 2.

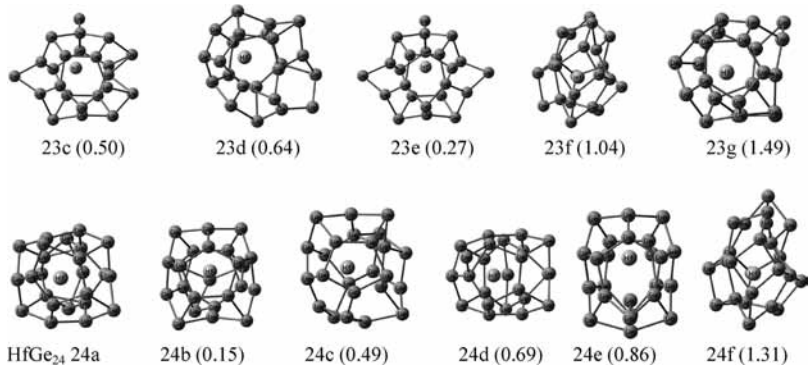

Figure 2. Part 2 of 2. The equilibrium structures of size-selective Hf@Ge$_n$ ($n = 18-24$). The relative energies (in eV) of the different isomers at the different sizes are shown in parentheses.

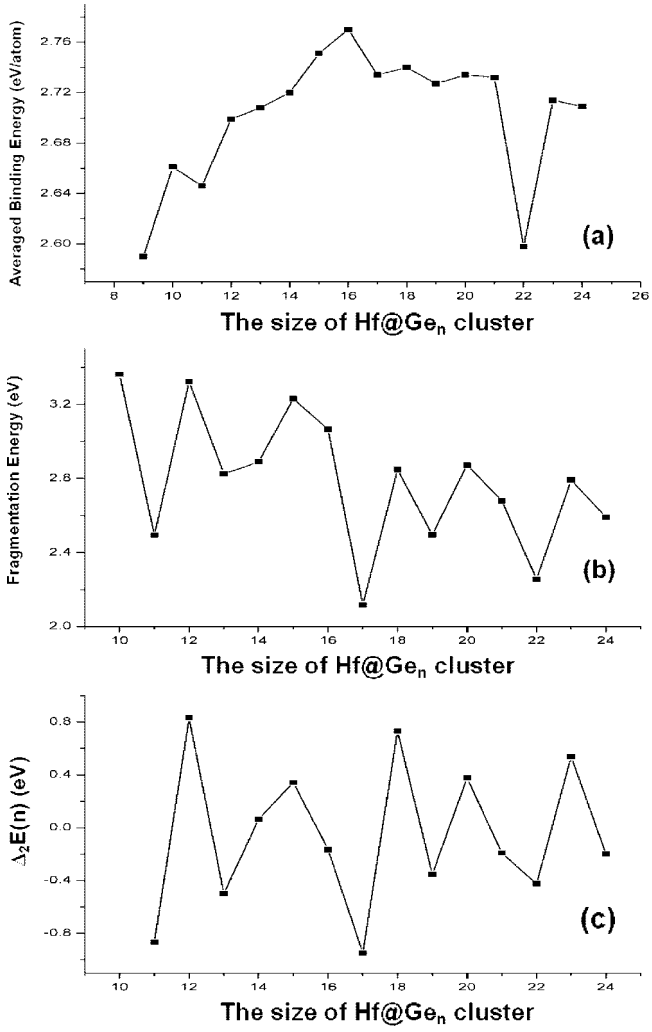

Figure 3. (a) Size dependence of the averaged atomic binding energies of Hf@Ge$_n$ clusters ($n = 9-24$). (b) Size dependence of the fragmentation energies of Hf@Ge$_n$ clusters ($n = 9-24$). (c) Size dependence of the second-order energy difference of Hf@Ge$_n$ clusters ($n = 9-24$).

the lowest-energy isomer and the dodecahedral isomer as the second-lowest-energy structure.

3.4. Electronic Properties of Size-Selective Hf@Ge$_n$ Clusters. In order to discuss the electron properties in the Hf@Ge$_n$ caged cluster, it is important to carry out natural bonding orbital (NBO) analysis and natural population analysis (NPA) to observe the natural charge populated on Hf; furthermore, the charge transfer mechanism between the impurity Hf and the germanium cage could be obtained. The natural charge populated on HfGe$_9$ is the lowest (−0.686) among the other size-selective caged Hf@Ge$_n$ clusters, suggesting that encapsulation of Hf in the germanium cage obviously absorbs the excess charges in the germanium framework, which is proven in the previous investigations on TMA-encapsulated silicon or germanium clusters.[5] However, it should be mentioned that the present investigation of wide size-selective Hf@Ge$_n$ ($n = 9-24$) suggests that the obvious difference in natural charges on Hf among the size-selective Hf@Ge$_n$ caged clusters is sensitive to the geometries of the isomers. For example, as illustrated in Table 1, the natural charges populated on the lowest-energy isomers of Hf@Ge$_{15}$ (−1.758) and Hf@Ge$_{16}$ (−2.169) are quite different from those of Hf@Ge$_{13}$ (−3.792) and Hf@Ge$_{14}$ (−3.400), which could be ascribed to the obvious difference among their geometries. The Hf@Ge$_{15}$ 15a and Hf@Ge$_{16}$ 16a are evolved from the pentagonal prism of Hf@Ge$_{10}$; hence, their natural charges on Hf are close to the pentagonal prism of Hf@Ge$_{10}$ (−1.885). As far as Hf@Ge$_{17}$ 17a is concerned, its natural charge on Hf (−3.015) is quite different from the lowest-energy Hf@Ge$_{16}$ 16a (−2.169) in that it is developed from fullerene-like Hf@Ge$_{16}$ 16b (−3.144). As for the lowest-energy isomers with sizes larger than 20, their natural charges on Hf are remarkably lower than that of Hf@Ge$_{20}$ 20a (−2.763) and close to that of dodecahedral Hf@Ge$_{20}$ 20b (−2.061), which indicates that dodecahedral could act as the precursor of large Hf@Ge$_n$ caged clusters. Therefore, it is concluded that charge

TABLE 1: The Lowest Vibrational Frequencies (in cm^{-1}), HOMO−LUMO Gaps (in eV), Natural Populated Charges on Doped Hf, Binding Energies (BE), Fragmentation Energies (FE), and the Second-Order Energy Differences of the Lowest-Energy Hf@Ge$_n$ Cage

caged cluster	Vf	HOMO−LUMO gap (eV)	Charges on Hf	BE (eV)	FE (eV)	$\Delta_2E(n)$ (eV)
Hf@Ge$_9$	29.8	1.566	−0.686	2.590		
Hf@Ge$_{10}$	46.3	2.709	−3.585	2.661	3.362	
Hf@Ge$_{11}$	32.4	1.985	−1.856	2.646	2.493	−0.869
Hf@Ge$_{12}$	34.6	1.896	−1.786	2.699	3.324	0.831
Hf@Ge$_{13}$	24.6	2.278	−3.792	2.708	2.825	−0.499
Hf@Ge$_{14}$	23.2	1.681	−3.4	2.72	2.889	0.064
Hf@Ge$_{15}$	38.0	1.711	−1.758	2.751	3.231	0.342
Hf@Ge$_{16}$	3.1	1.995	−2.169	2.77	3.065	−0.166
Hf@Ge$_{17}$	38.3	1.493	−3.015	2.734	2.116	−0.949
Hf@Ge$_{18}$	39.1	1.70	−2.871	2.74	2.848	0.732
Hf@Ge$_{19}$	28.8	1.629	−2.653	2.727	2.495	−0.353
Hf@Ge$_{20}$	40.7	1.546	−2.763	2.734	2.872	0.377
Hf@Ge$_{21}$	35.1	1.429	−1.287	2.732	2.68	−0.192
Hf@Ge$_{22}$	36.3	1.378	−1.204	2.598	2.255	−0.425
Hf@Ge$_{23}$	33.6	1.491	−2.071	2.714	2.791	0.536
Hf@Ge$_{24}$	30.0	1.602	−1.974	2.709	2.591	−0.2

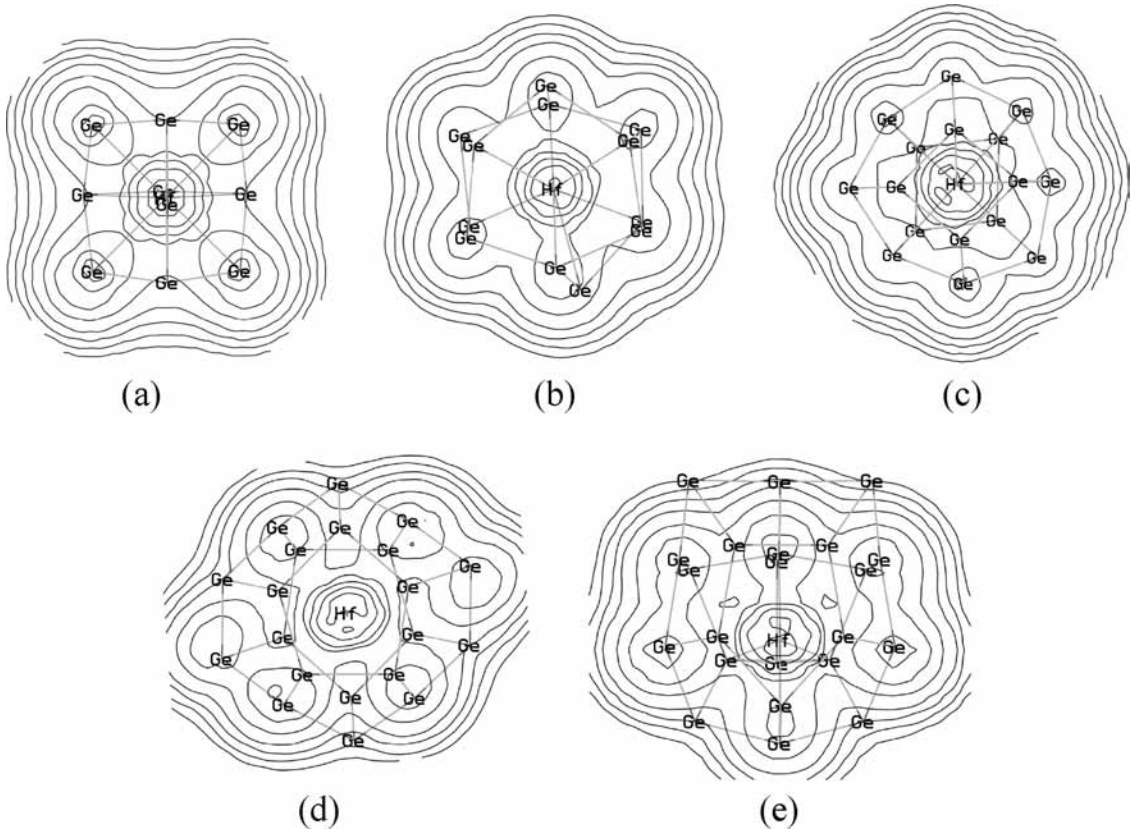

Figure 4. The topography of total electronic densities on the plane (isovalue is 0.008) of Hf@Ge_n cage. (a) $HfGe_{10}$ 10a; (b) $HfGe_{12}$ 12a hexagonal prism; (c) $HfGe_{16}$ 16b fullerene-like cage; (d) $HfGe_{20}$ dodecahedral cage; (e) $HfGe_{22}$ 22b.

distribution between Hf and a germanium cage is determined by the growth behavior of Hf@Ge_n clusters.

The large HOMO−LUMO gaps of the pentagonal prism of Hf@Ge_{10} (1.835 eV), the hexagonal prism of Hf@Ge_{12} (1.896 eV), the fullerene-like cage of Hf@Ge_{16} (1.737 eV), and the dodecahedral cage of Hf@Ge_{20} (1.803 eV) indicate that these species could be considered as the templates or building-blocks of 1D or 3D structures of Hf-doping nanoclusters. As mentioned above, the averaged binding energy of size-selective Hf@Ge_n suggests that binding energy gradually increases to the maximum and tends to be decreased subsequently after Hf@Ge_{16}. As illustrated in Table 1, the HOMO−LUMO gaps of size-selective Hf@Ge_n ($n = 17-24$) is distinctly lower than those of Hf@Ge_n ($n = 10-16$), suggesting that when the cluster size of Hf@Ge_n is more than 16, the germanium cage needs to be stabilized by more Hf impurities to directly interact with germanium atoms in the outer layer. According to the previous gas-phase experiment of single TMA-doped silicon or germanium clusters, obvious intensity could be only observed at sizes lower than 16 in mass spectrometry.[1,2] Moreover, the mass spectrum of a Hf-doped silicon cluster reveals that the prominent peak appears at 16, suggesting that the binding energy of $HfSi_{16}$ is very strong compared to other size-selective $HfSi_n$ clusters. In the case of a Hf@Ge_n cluster, the binding energy of Hf@Ge_{16} is also the strongest, which is similar to the mass spectrum of $HfSi_n$ and can be explained by the octet (18 electrons) rule. In addition, the threshold size of the adsorption reactivity of neutral $HfSi_n$ toward H_2O is indicated at $n = 14$, indicating that the formation of a Hf-encapsulated silicon cage causes the loss of reactivity.[2] In the case of Hf@Ge_n, the smallest fullerene-like structure could be located at $n = 14$, which is analogous to the prediction about the geometry of $HfSi_n$ in the experiment.[2] Similar to pure Ge_n clusters,[27] HOMO−LUMO gaps tend to be oscillated and gradually decreased in Hf@Ge_n clusters.

TABLE 2: Comparison between a Low-Lying Size-Selective Empty Si_n Cage, Hf@Si_n, and an Empty Ge_n cage, Hf@Ge_n

caged clusters	BE (eV)[a]	EE (eV)[b]	HOMO−LUMO gap (eV)	charges populated on Hf
hexagonal Si_{12}	2.662		1.518	
hexagonal Hf@Si_{12}	3.007	7.149	1.720	−3.290
fullerene-like Si_{16}	2.816		1.705	
fullerene-like Hf@Si_{16}	3.248	10.173	2.109	−3.372
dodecahedral Si_{20}	2.866		1.348	
dodecahedral Hf@Si_{20}	3.187	9.617	1.300	−2.230
hexagonal Ge_{12}	2.409		1.545	
hexagonal Hf@Ge_{12}	2.699	6.167	1.896	−1.786
fullerene-like Ge_{16}	2.474		1.956	
fullerene-like Hf@Ge_{16}	2.756	7.264	1.737	−3.144
dodecahedral Ge_{20}	2.478		1.489	
dodecahedral Hf@Ge_{20}	2.729	7.740	1.803	−2.061

[a] $BE = nE(X) + E(Hf) - E(Hf@X_n)/n + 1$ (X = Si or Ge), and $BE = nE(X) - E(X_n)/n$ (X = Si or Ge). [b] $EE = E(X_n) + E(Hf) - E(Hf@X_n)$ (X = Si or Ge) (EE is embedding energy).

As shown from topography (in Figure 4) of electronic density distribution in the lowest-energy 10a, the electron charge density is mainly distributed around partial Ge atoms, and weak interaction could be formed between Hf and these Ge atoms. In the case of hexagonal prism Hf@Ge_{12}, covalent bonding among some Ge atoms could be formed, and no electron charge density can be observed on four Ge atoms, suggesting the formation of covalent bonding in the four Ge atoms and that Hf is doped in the Ge atoms of the open cage. Furthermore, the covalent bonding at the bottom of Ge atoms is obviously attracted toward the Hf atom and appears to have covalent

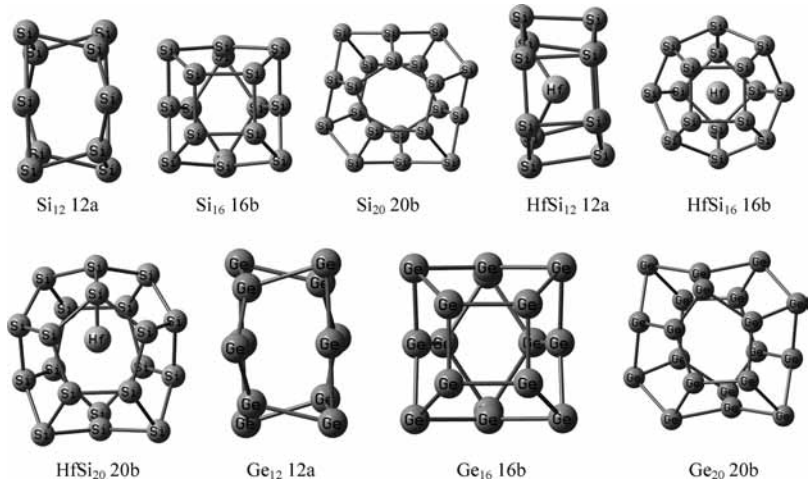

Figure 5. The equilibrium structures for low-lying isomers of hexagonal cage Hf@Si_{12}, fullerene-like cage Hf@Si_{16}, and dodecahedral cage Hf@Si_{20} with their corresponding empty silicon cages. The equilibrium geometries of empty hexagonal cage Ge_{12}, fullerene-like cage Ge_{16}, and dodecahedral cage Ge_{20} with their Hf-encapsulated cages referring to Figures 11 and 22.

metallic character. The unbalanced interaction between Hf and the Ge framework leads to the distortion structure of a hexagonal prism, which is reflected by the different bond lengths of Hf−Ge in the optimized geometry. As seen from the topography of electron density in fullerene-like Hf@Ge_{16}, there is a remarkable electron charge between Hf and the eight Ge atoms in the rhombii antiprsim, implying that the eight capped Ge atoms can form the outer layer, and very weak interaction exists in the encapsulated Hf and the eight Ge atoms. Compared to fullerene-like Hf@Ge_{16}, very low electron density between Hf and the pentagonal antiprism of germanium reveals that no obvious interaction between Hf and germanium located at the inner layer could be formed; furthermore, covalent bonding between Hf in the pentagon and partially capped germanium atoms is almost located along the axis between Ge atoms without the effects from the Hf atom. As seen from topography of electron density in the analogous low-lying dodecahedral Hf@Ge_{22} 22b, there is strong interaction between the inserted Ge atom in the pentagonal antiprism and Hf. Because Hf is moved away from the center of cage in Hf@Ge_{22} 22b, no interaction between the three germanium atoms at the top of the cage and the other Ge atoms or Hf could be formed, which is reflected by the contour level of the Ge atoms at the top of the cage being lower than that of the Ge atoms at the bottom of cage. Therefore, the topography of the electronic density distribution and covalent bonding of germanium atoms in size-selective Hf@Ge_n is mainly dependent on the encapsulated position of Hf in the cage and the shape of the germanium framework.

3.5. Comparison between Size-Selective Hf-Encapsulated Germanium and Silicon Cage. In order to investigate the encapsulating effect of Hf in a germanium cage in comparison with a silicon cage, some typical low-lying isomers, e.g., the hexagonal prism of Hf@X_{12}, the fullerene-like structure of Hf@X_{16}, and the dodecahedral cage of Hf@X_{20} (X = Si and Ge) are considered to be optimized in the present work. Additionally, the empty germanium or silicon clusters, i.e., hexagonal prism X_{12}, fullerene-like structure of X_{16} and dodecahedral cage of X_{20} (X = Si and Ge), are also optimized so that alteration in some characteristics of empty silicon or germanium cage, that is, embedding energy, binding energy, or energy gap in the frontier orbital, could be discussed when single Hf is encapsulated in the pure silicon or germanium cage.

As far as the hexagonal prism Hf@X_{12} (X = Si and Ge) is concerned, the embedding energy (7.149 eV) of Hf@Si_{12} and binding energy (3.007 eV) of Hf@Si_{12} cage are obviously higher than the embedding energy of Hf@Ge_{12} (6.617 eV) and binding energy of Hf@Ge_{12} (2.699 eV), respectively, suggesting that that obvious strong interaction between Hf and the silicon cage contributes to strengthening the stability of Hf@Si_{12} compared to Hf@Ge_{12}. Moreover, larger charge reversing from the Si_{12} cage to Hf (−3.290) compared to that from the Ge_{12} cage to Hf (−1.786) indicates more efficient dispersion of excess charge in the Si_{12} cage when Hf is encapsulated in silicon hexagonal prism and implies that sp^2 hybridization of silicon atoms in this cage could be easily formed in comparison with the germanium cage. That is the reason why the metal-encapsulated Si_{12} cluster could be much easier to be observed compared to the metal-encapsulated Ge_{12} cluster in the previous experiments.[1,12]

In the case of fullerene-like Hf@Ge_{16} 16b, its embedding energy (7.264 eV) is remarkably lower than that of fullerene-like Hf@Si_{16} (10.173 eV) (refer to Table 2). On the other hand, the binding energy can be increased by 0.432 eV if Hf is encapsulated in the Si_{16} cage; however, the binding energy of fullerene-like Hf@Ge_{16} (2.756 eV) is only higher than that of empty fullerene-like Ge_{16} (2.474 eV) by 0.282 eV. As far as the HOMO−LUMO gap is concerned, the HOMO−LUMO gap (1.705 eV) of empty Si_{16} will be distinctly increased to 2.109 eV if Hf is encapsulated in the Si_{16} cage. On the contrary, when Hf is encapsulated in the Ge_{16} cage, the HOMO−LUMO gap of empty Ge_{16} (1.956 eV) is significantly decreased to be 1.737 eV. Therefore, it can be concluded that the stability of fullerene-like Hf@Ge_{16} is relatively low compared to the analogous isomer Hf@Si_{16}, implying that the growth behavior of a Hf-encapsulated silicon cage is different from that of a Hf-encapsulated germanium cage. That is the reason why fullerene-like Zr@Si_{16} is the lowest-energy structure,[29] whereas the analogous fullerene-like Hf@Ge_{16} is the second-lowest-energy structure; furthermore, it can be expected that the growth behavior of a single metal encapsulated silicon cage is different from that of single metal encapsulated germanium cage.

Compared to the high embedding energy of fullerene-like Hf@Si_{16} (10.173 eV) (see Table 2), the embedding energy of dodecahedral Hf@Si_{20} is decreased to be (9.617 eV); however, dodecahedral Hf@Ge_{20} has relatively high embedding energy (7.740 eV) compared to that of fullerene-like Hf@Ge_{16} (7.264 eV). In addition, the HOMO−LUMO gap (1.300 eV) of dodecahedral Hf@Si_{20} is slightly lower than that of empty dodecahedral Si_{20} (1.348 eV), whereas the HOMO−LUMO gap

of empty dodecahedral Ge_{20} (1.489 eV) is obviously increased by 0.314 eV when Hf is encapsulated in the empty dodecahedral Ge_{20} cage. As shown from optimized geometry of the dodecahedral $Hf@Si_{20}$ in Figure 5, Hf is moved from the center of dodecahedral cage and obviously bonded with the top Si atom corresponding to a Hf−Si bond length of 2.763 Å; however, in the case of the dodecahedral $Hf@Ge_{20}$ cage, Hf is still encapsulated in the center of the dodecahedral Ge_{20} cage, suggesting that the encapsulated behavior of Hf in a dodecahedral Ge_{20} cage is different from that in a dodecahedral Si_{20} cage, which contributes to forming a divergence between the geometries of $Hf@Ge_{20}$ and $Hf@Si_{20}$.

To sum up, the present comparison between some low-lying isomers of $Hf@Si_n$ and $Hf@Ge_n$ clusters suggests that obvious divergences, e.g., stabilities, growth behavior, and electronic properties, can be found. Considering that very limited present experimental observation of metal encapsulated germanium nanoclusters and quite unsystematically theoretical investigation on metal encapsulated germanium nanoclusters in the range of 16 to 24 have been done, it is necessary to give a thorough study on the growth behavior and electronic properties of large Hf-encapsulated germanium cages.

4. Conclusion

The geometries, relative stabilities, and electronic properties of size-selective $Hf@Ge_n$ ($n = 9-24$) caged clusters are investigated using the UB3LYP/LanL2DZ method. All of the results can be summarized as follows:

(1) Compared to the hexagonal prism of $Hf@Ge_{12}$, the pentagonal prism is more favorable to form solid a Hf-encapsulated germanium cage. The fullerene-like $Hf@Ge_{16}$ and dodecahedral $Hf@Ge_{20}$ with large HOMO−LUMO gap are suggested as the candidates for the most stable structure at that size. When the size of $Hf@Ge_n$ is larger than 20, the encapsulated position of Hf is obviously distorted from the center of the germanium cage, and some germanium atoms begin to form an outer layer, which is not directly interacted with Hf. Therefore, in order to stabilize the solid germanium cage, more Hf impurities should be encapsulated in the cage.

(2) The binding energy of size-selective $Hf@Ge_n$ increases to the maximum at $n = 16$, then gradually decreases with the increase of the cluster size from 16 to 24, which is analogous to the experimental observations of $Hf@Si_n$. The magic number of size-selective $Hf@Ge_n$ appears at 10, 12, 15, 16, 18, 20, and 23, implying that these size-selective clusters have special stability and could be possibly observed in laser vaporization gas phase experiments. Furthermore, the magic number of $Hf@Ge_n$ is somewhat different from that of pure Ge_n clusters, which suggests that doping of single Hf in a germanium cage cause the selectivity of the relative stability of different sizes.

(3) The large HOMO−LUMO gaps of the pentagonal prism of $Hf@Ge_{10}$, the hexagonal prism of $Hf@Ge_{12}$, the fullerene-like cage of $Hf@Ge_{16}$, and the dodecahedral cage of $Hf@Ge_{20}$ suggest that these species could be considered as the templates or building-blocks of 1D or 3D structures of Hf doping nanoclusters.

(4) The present comparison between low-lying size-selective $Hf@Ge_n$ and $Hf@Si_n$ cages reveals that large-scaled divergence in some properties, viz., growth behaviors, binding energies, embedding energies, and electronic properties, have been found between the two kinds of nanoclusters.

Acknowledgment. This work is supported by National Basic Research Program of China (2007CB936603) and the National Natural Science Foundation of China (60574094, 60574095, 10635070).

References and Notes

(1) Hiura, H.; Miyazaki, T.; Kanayama, T. *Phys. Rev. Lett.* **2001**, *86*, 1733.

(2) Kayasu, K.; Atobe, J.; Akutsu, M.; Mitsui, M.; Nakajima, A. J. *Phys. Chem. A.* **2007**, *111*, 42.

(3) Ohara, M.; Koyasu, K.; Nakajima, A.; Kaya, K. *Chem. Phys. Lett.* **2003**, *371*, 490.

(4) Jaeger, J. B.; Jaeger, T. D.; Duncan, M. A. *J. Phys. Chem. A.* **2006**, *110*, 9310.

(5) (a) Wang, J.; Han, J. G. *J. Chem. Phys.* **2005**, *123*, 244303. (b) Wang, J.; Han, J. G. *J. Phys. Chem. B* **2006**, *110*, 7820. (c) Wang, J.; Han, J. G. *Chem. Phys.* **2007**, *342*, 253.

(6) (a) Lu, J.; Nagase, S. *Phys. Rev. Lett.* **2003**, *90*, 115506. (b) Lu, J.; Nagase, S. *Chem. Phys. Lett.* **2003**, *372*, 394.

(7) Chuang, F. C.; Hsieh, Y. Y.; Hsu, C. C.; Albao, M. A. *J. Chem. Phys.* **2007**, *127*, 144313.

(8) Peng, Q.; Shen, J. *J. Chem. Phys.* **2008**, *128*, 084711.

(9) Sporea, C.; Rabilloud, F. *J. Chem. Phys.* **2007**, *127*, 164306.

(10) Kawamura, H.; Kumar, V.; Kawazoe, Y. *Phys. Rev. B.* **2005**, *71*, 075423.

(11) Kumar, V.; Kawazoe, Y. *Appl. Phys. Lett.* **2003**, *83*, 2677.

(12) Zhang, X.; Li, G. L.; Gao, Z. *Rapid. Commun. Mass. Spectrom.* **2001**, *15*, 1573.

(13) Kumar, V.; Kawazoe, Y. *Appl. Phys. Lett.* **2002**, *80*, 859.

(14) Singh, A. K.; Kumar, V.; Kawazoe, Y. *Phys. Rev. B.* **2004**, *69*, 233406.

(15) Zhao, R. N.; Ren, Z. Y.; Guo, P.; Bai, J. T.; Zhang, C. H.; Han, J. G. *J. Phys. Chem. A* **2006**, *110*, 4071.

(16) Guo, P.; Ren, Z. Y.; Yang, A. P.; Han, J. G.; Bian, J.; Wang, G. H. *J. Phys. Chem. A* **2006**, *110*, 7453.

(17) Han, J. G.; Ren, Z. Y.; Lu, B. Z. *J. Phys. Chem. A* **2004**, *108*, 5100.

(18) Kumar, V.; Singh, A. K.; Kawazoe, Y. *Phys. Rev. B* **2006**, *74*, 125411.

(19) Singh, A. K.; Kumar, V.; Kawazoe, Y. *Phys. Rev. B* **2005**, *71*, 115429.

(20) Singh, A. K.; Kumar, V.; Kawazoe, Y. J. *Phys. Chem. A* **2005**, *109*, 15187.

(21) Kumar, V.; Briere, T. M.; Kawazoe, Y. *Phys. Rev. B* **2003**, *68*, 155412.

(22) Becke, A. D. *Phys. Rev. A* **1988**, *38*, 3098.

(23) Lee, C.; Yang, W.; Parr, R. G. *Phys. Rev. B* **1988**, *27*, 785.

(24) Wadt, W. R.; Hay, P. J. *J. Chem. Phys.* **1985**, *82*, 284.

(25) Hu, Z.; Dong, J. G.; Lombardi, J. R.; Lindsay, D. M. *J. Phys. Chem.* **1993**, *97*, 9263.

(26) Frisch, M. J.; Trucks, G. W.; Schlegel, H. B.; Scuseria, G. E.; Robb, M. A.; Cheeseman, J. R.; Montgomery, J. A., Jr.; Vreven, T.; Kudin, K. N.; Burant, J. C.; Millam, J. M.; Iyengar, S. S.; Tomasi, J.; Barone, V.; Mennucci, B.; Cossi, M.; Scalmani, G.; Rega, N.; Petersson, G. A.; Nakatsuji, H.; Hada, M.; Ehara, M.; Toyota, K.; Fukuda, R.; Hasegawa, J.; Ishida, M.; Nakajima, T.; Honda, Y.; Kitao, O.; Nakai, H.; Klene, M.; Li, X.; Knox, J. E.; Hratchian, H. P.; Cross, J. B.; Bakken, V.; Adamo, C.; Jaramillo, J.; Gomperts, R.; Stratmann, R. E.; Yazyev, O.; Austin, A. J.; Cammi, R.; Pomelli, C.; Ochterski, J. W.; Ayala, P. Y.; Morokuma, K.; Voth, G. A.; Salvador, P.; Dannenberg, J. J.; Zakrzewski, V. G.; Dapprich, S.; Daniels, A. D.; Strain, M. C.; Farkas, O.; Malick, D. K.; Rabuck, A. D.; Raghavachari, K.; Foresman, J. B.; Ortiz, J. V.; Cui, Q.; Baboul, A. G.; Clifford, S.; Cioslowski, J.; Stefanov, B. B.; Liu, G.; Liashenko, A.; Piskorz, P.; Komaromi, I.; Martin, R. L.; Fox, D. J.; Keith, T.; Al-Laham, M. A.; Peng, C. Y.; Nanayakkara, A.; Challacombe, M.; Gill, P. M. W.; Johnson, B.; Chen, W.; Wong, M. W.; Gonzalez, C.; Pople, J. A. *Gaussian 03*; Gaussian, Inc.: Pittsburgh, PA, 2003.

(27) Wang, J. L.; Wang, G. H.; Zhao, J. *Phys. Rev. B* **2001**, *64*, 205411.

(28) Kawamura, H.; Kumar, V.; Kawazoe, Y. *Phys. Rev. B* **2004**, *70*, 245433.

(29) Wang, J.; Han, J. G. *J. Chem. Phys.* **2005**, *123*, 064306.

(30) Singh, A. K.; Kumar, V.; Kawazoe, Y. J. *Mater. Chem.* **2004**, *14*, 555.

JP804433D